Soil Dynamics and Earthquake Engineering 163 (2022) 107532

Contents lists available at ScienceDirect

Soil Dynamics and Earthquake Engineering

journal homepage: www.elsevier.com/locate/soildyn

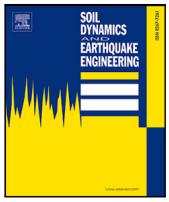

Analytical 1D transfer functions for layered soils

Joaquin Garcia-Suarez [a,*], Javier González-Carbajal [b], Domniki Asimaki [c]

[a] Institute of Civil Engineering, Institute of Materials, École Polytechnique Fédérale de Lausanne (EPFL), CH-1015 Lausanne, Switzerland
[b] Department of Mechanical Engineering and Manufacturing, University of Seville, Spain
[c] Department of Mechanical and Civil Engineering, California Institute of Technology, Pasadena, CA, USA

ARTICLE INFO

Keywords:
Elasticity
Geotechnical earthquake engineering
Inverse analysis
Layered soils
Seismology
Site response analysis
Transfer function

ABSTRACT

Transfer functions are constantly used in both Seismology and Geotechnical Earthquake Engineering to relate seismic ground motion at different depths within strata. In the context of diffusive theory, they also appear in the expression of the imaginary part of 1D Green's functions. In spite of their remarkable importance, their mathematical structure is not fully understood yet, except in the simplest cases of two or three layers at most. This incomplete understanding, in particular as to the effect of increasing number of layers, hinders progress in some areas, as researchers have to resort to expensive and less conclusive numerical parametric studies. This text presents the general form of transfer functions for any number of layers, overcoming the above issues. The mathematical structure of these transfer functions comes defined as a superposition of independent harmonics, whose number, amplitudes and periods we fully characterize in terms of the properties of the layers in closed-form. Owing to the formal connection between seismic wave propagation and other phenomena that, in essence, represent different instances of wave propagation in a linear-elastic medium, we have extended the results derived elsewhere, in the context of longitudinal wave propagation in modular rods, to seismic response of stratified sites. The ability to express the reciprocal of transfer functions as a superposition of independent harmonics enables new analytical approaches to assess the effect of each layer over the overall response. The knowledge of the general closed-form expression of the transfer functions allows to analytically characterize the long-wavelength asymptotics of the horizontal-to-vertical spectral ratio for any number of layers.

1. Introduction

The study of elastic-wave propagation phenomena is of utmost interest to both the seismology and the geotechnical earthquake engineering communities: the sudden release of energy created by a fault rupturing generates a deformation field that propagates towards the free surface and it is ultimately felt as an earthquake. This wavefield is usually studied using the tools of linear elasticity [1], except when the propagation takes place within soft soils, what requires considering material non-linear response [2]. It is also the case that when the front arrives to the shallow layers, assuming the earthquake source is located deep enough, it does so almost-vertically (the decreasing stiffness bends the rays towards the normal of the free surface) [1]. Moreover, for the length-scales of interest in applications, the local curvature of the wavefield is relatively small compared to the window of observation, so the impinging excitation can be considered to be made up of plane waves, ignoring the curvature of the fronts.

Under the assumptions of one-dimensional propagation perpendicular to the free surface and linear response, the different components decouple and SH, SV and P waves can be studied separately and then summed up, as there is no mode conversion.

A customary method to study the evolution of the wave fields across the layers is the so-called "propagator matrix method", also referred as "method of matrizants" in older texts [3]. An equivalent matrix approach for the 1D case is presented in [2], and it is used in geotechnical engineering often. The classic seismology texts [1,4] present a general treatment for inclined SH waves and inclined P-SV waves; however, in this work, following Ref. [5], we will consider no inclination, thus the expressions that appear in the prior references can be simplified.

These approaches based on propagator matrices assign a matrix to every layer in the site, which depends on the mechanical properties of the material the layer is made of as well as on the ratio between the wavelength of the propagating plane wave to the thickness of the layer. These matrices link stresses and displacements in one border of the layer to the other one. Among other usages, this method allows obtaining "transfer functions" to relate the displacement amplitude at the free surface to either the displacement at a deeper stratum or to

* Corresponding author.
E-mail address: joaquin.garciasuarez@epfl.ch (J. Garcia-Suarez).

https://doi.org/10.1016/j.soildyn.2022.107532
Received 19 June 2022; Received in revised form 5 September 2022; Accepted 5 September 2022
Available online 24 September 2022

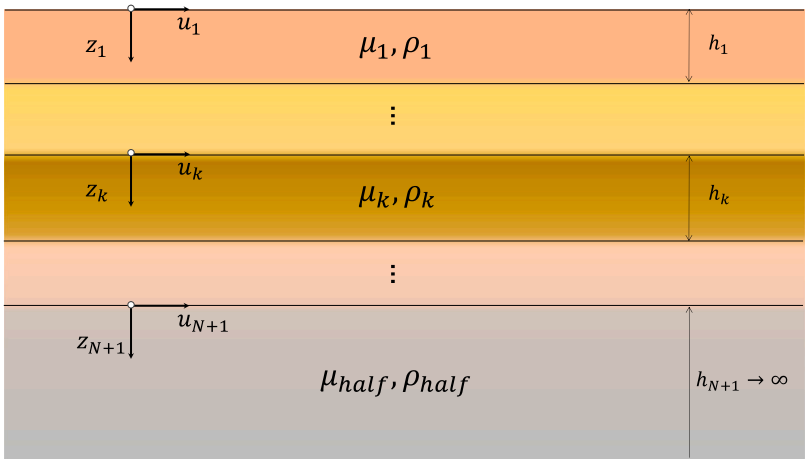

Fig. 1. Scheme of the layered system and local coordinates. μ_i, ρ_i $(i = 1, 2, \ldots, N)$ represent respectively the shear modulus and the density of the ith layer, while those of the half-space are termed μ_{half}, ρ_{half}; u_i, h_i, z_i $(i = 1, 2, \ldots, N+1)$ represent respectively the horizontal deformation induced by the shear wave, the thickness and the local vertical coordinate (stretching from top to bottom) of the ith layer, the $N+1$ layer corresponds to the half-space (thus its thickness is assumed infinite).

the amplitude of the wave that impinges on the shallow layers coming from an idealized half-space (typically referred to as the incident wave at the top of the elastic bedrock).

Even though these transfer functions are usually obtained numerically, there is still room for closed-form analysis. The general expression for transfer functions in sites with any number of layers is presented and then verified against numerical evaluation following the usual numerical matrix-multiplication procedure. Finally, a relevant application of the new closed-form formulae is explored: obtaining analytical expression for the ratio between horizontal and vertical spectral surface amplitude components in the long-wavelength limit, following the example of Kawase and colleagues [5].

Before concluding this introduction, let us mention that the elastic wave propagation in layered media is of interest to the solid mechanics community at large, in particular, also to researchers interested in dispersion relations in periodic structures [6,7]. It is in this context that the general form of the N-layer propagator has recently been introduced [8]. The mathematical problem is the same in both cases, despite its guise being different. Since the derivation of the general form of the entries of the global propagator is presented in Ref. [8], it will not be included in the text and the reader interested in such details is referred to that publication. Beyond elasticity, electromagnetic waves [9] and acoustic waves [10] propagating in layered media in 1D fashion also adopt a similar mathematical form.

2. Closed-form expression of general transfer functions

2.1. Brief refresh of the mathematical modeling

A reader interested in thorough treatment of the subject is referred to Aki and Richards' book [1].

Let us illustrate the method using S waves at first, yet considering P waves instead only requires swapping the medium shear modulus with the corresponding modulus. We assume that the Fourier transform has been applied to the equations of the problem, thus the results are given in the frequency domain. The method considers balance of linear momentum (equilibrium) and the constitutive relation (relation stress–strain). Under the 1D assumption, frequency-domain, for S waves, these equations in matrix form read as (see Section 5.4. in Ref. [1]):

$$\frac{d\boldsymbol{f}}{dz} = \frac{d}{dz}\begin{bmatrix}\hat{u}\\ \hat{\tau}_{xz}\end{bmatrix} = \begin{bmatrix}0 & 1/\mu_k\\ -\rho_k\omega^2 & 0\end{bmatrix}\begin{bmatrix}\hat{u}\\ \hat{\tau}_{xz}\end{bmatrix} = \boldsymbol{A}_k\boldsymbol{f}(z), \tag{1}$$

where z is the vertical coordinate, see Fig. 1, $\hat{u}$ represents the Fourier-amplitude (frequency-domain amplitude) of the horizontal displacement, $\hat{\tau}_{xz}$ is the amplitude of the shear stresses, μ_k and ρ_k refer respectively to the shear modulus and the density of the soil, and ω is the circular frequency of the propagating wave. Later on, we will include the effect of hysteretic damping in the soil, hence we will use the symbol $\delta_{d,k}$ to refer to the damping coefficient of the kth layer (recall that, invoking the Equivalence Principle [4], introducing this kind of dissipation mechanism in the frequency-domain response of the material amounts to substituting the real shear modulus μ_k by a complex one given by $\mu_k(1 + \mathrm{i}\delta_{d,k})$).

We assume that conditions at the surface of the site are given by $\boldsymbol{f}(z = 0) = [\hat{u}_{top}, 0]^\top$, where $\hat{u}_{top}$ is the unknown ground displacement and the stress is zero as there are no forces imposed on this contour. The vector $\boldsymbol{f}$ is called the motion-stress vector, the matrix $\boldsymbol{A}_k$ is referred to as the kth layer matrix. For a given frequency, the matrix layer is a constant within the layer as mechanical properties remain constant themselves.

2.2. Transfer functions

To conclude with the review, we remind the reader of the two kinds of transfer functions that appear profusely in the literature.

2.2.1. Surface-to-borehole ground motion

The stress-free surface translates into a zero entry of the motion-stress vector at $z = z_0 = 0$:

$$\boldsymbol{f}(0) = [\hat{u}_{top} \quad 0]^\top. \tag{2}$$

This means that the relation between the displacement at the free-surface, $\hat{u}_{top}$ and the displacement at the $N+1$ interface, assumed to be the interface where the last layer meets the half-space, comes given by

$$\boldsymbol{f}(z = z_{N+1}) = \begin{bmatrix}\hat{u}\\ \hat{\tau}_{xz}\end{bmatrix}_{z=z_{N+1}} = \boldsymbol{P}(z_{N+1}, z_0)\begin{bmatrix}\hat{u}_{top}\\ 0\end{bmatrix}$$
$$\to TF_{u-u}(\omega) = \frac{\hat{u}_{top}}{\hat{u}_b} = \frac{1}{P_{11}(z_{N+1}, z_0)}, \tag{3}$$

the displacement at the base (interface with the half-space) is $\hat{u}_b = \hat{u}(z = z_{N+1})$.

2.2.2. Surface-to-incident ground motion

Let us focus on the last layer overlying the half-space. This expression has also been considered in the past [5,11]. The displacement at the base of the last layer is equal to the one at the top of the half-space, which in turn is given by the superposition of the impinging wave and the transmitted back into the half-space after traversing the

upper strata back and forth. Following the traditional seismological notation, $\acute{S}$ represents the upward-going wave amplitude, while $\grave{S}$, the down-going one. Thus, we can write the base-to-top relation as

$$\boldsymbol{f}(z=z_{N+1}) = \begin{bmatrix} \hat{u} \\ \hat{\tau}_{xz} \end{bmatrix}_{z=z_{N+1}} = \begin{bmatrix} \grave{S}+\acute{S} \\ \mu_{half}\,\mathrm{i}k(\acute{S}-\grave{S}) \end{bmatrix}_{z=z_{N+1}} = \boldsymbol{P}(z_{N+1}x, z_0)\begin{bmatrix} \hat{u}_{top} \\ 0 \end{bmatrix} = \begin{bmatrix} P_{11}\hat{u}_{top} \\ P_{21}\hat{u}_{top} \end{bmatrix}, \tag{4}$$

thus the ratio $\hat{u}_{top}/\acute{S}$ can be written as

$$\mathrm{TF}(\omega) = \frac{\hat{u}_{top}}{\acute{S}} = \frac{2}{P_{11} - \mathrm{i}\frac{P_{21}}{\omega\sqrt{\rho_{half}\mu_{half}}}}. \tag{5}$$

Let us state the obvious relation between the two transfer functions:

$$\frac{2}{\mathrm{TF}} = \frac{1}{TF_{u-u}} - \mathrm{i}\frac{P_{21}}{\omega\sqrt{\rho_{half}\mu_{half}}}. \tag{6}$$

Notice that the subscript "$u-u$" and italic font are being used to distinguish one transfer function from the other. Later in the text, the subscript "p" and "s" will be attached to TF to clarify if its refer to either pressure or shear wave propagation.

2.3. General expression for surface-to-borehole transfer function

As mentioned above, the detailed derivation of the general form of the global propagator can be consulted in Ref. [8]. Since the upcoming results make extensive use of multi-index notation, the Supplementary Material contains a brief review of the subject.

The general term for the displacement-to-displacement transfer function, in a site with N layers, is [8]

$$TF_{u-u}(\omega)^{-1} = \sum_{k=1}^{2^{N-1}} 2A_k \cos\left(\tau_k\omega\right), \tag{7}$$

where the discrete spectrum of the inverse if the transfer function is fully defined by the characteristic "spectral periods" of the N-layer site, given by

$$\tau_j = \left[\frac{h_1}{c_1}, \ldots, \frac{h_N}{c_N}\right]^{\mathsf{T}} \cdot \mathbf{e}_j, \tag{8}$$

where the jth permutation vector $\mathbf{e}_j \in \{-1, 1\}^N$ can be any element in the set satisfying $\mathsf{e}_{j,1} = 1$ (see that there are 2^{N-1} elements in this subset and that $\mathsf{e}_{j,1}$ refers to the first element of the jth permutation vector), while the "spectral amplitude" corresponding to $\mathbf{e}_j$ is

$$A_j = \frac{1}{2^N}\sum_{k=0}^{\lfloor N/2\rfloor}\sum_{|\mathsf{b}|=2k}(-1)^{k+\frac{\mathsf{b}\cdot\mathbf{e}_j}{2}}(\sqrt{\rho\mu})^{\mathrm{f}(\mathsf{b})}, \tag{9}$$

each binary multi-index [12] $\mathsf{b} \in \{0, 1\}^N$ codifies the effect of the impedance contrast at the interfaces, and the map $\mathrm{f} : \{0, 1\}^N \to \{-1, 0, 1\}^N$ takes the multi-index b, entry-wise, to the multi-index $\mathrm{f}(\mathsf{b})$ defined as:

- if $\mathsf{b}_i = 0$, then $\mathrm{f}(\mathsf{b}_i) = 0$,
- if $\mathsf{b}_i = 1$ and it is the first instance of an entry being equal to 1, then $\mathrm{f}(\mathsf{b}_i) = 1$.
- if $\mathsf{b}_i = 1$ and the previous value assigned by f to the prior 1-entry in b was -1, then $\mathrm{f}(\mathsf{b}_i) = 1$, else $\mathrm{f}(\mathsf{b}_i) = -1$.

There is another form of writing Eq. (7) [8], one which is more convenient when it comes to study long-wavelength asymptotics (Section 4)

$$TF_{u-u}(\omega)^{-1} = \left(\prod_{i=1}^{N}\cos(r_i)\right)\left(\sum_{\beta=0}^{\lfloor N/2\rfloor}\sum_{|\mathsf{b}|=2\beta} C_{\mathsf{b}}\tan(r)^{\mathsf{b}}\right), \tag{10}$$

where $\lfloor\cdot\rfloor$ is the floor function, $r_i = \omega h_i/\sqrt{\mu_i/\rho_i}$, the coefficients C_{b} being given by

$$C_{\mathsf{b}} = (-1)^{|\mathsf{b}|/2}(\sqrt{\rho\mu})^{\mathrm{f}(\mathsf{b})}, \tag{11}$$

where $\mathrm{f}(\mathsf{b})$ was introduced following Eq. (9). The total number of addends in the sum Eq. (10) (each addend being a product of certain number of tangents except for the first one that is simply 1) is equal to

$$N_{addends} = 1+\binom{N}{2}+\binom{N}{4}+\ldots+\binom{N}{\lfloor N/2\rfloor} = \sum_{k=1}^{\frac{1}{2}\lfloor N/2\rfloor}\binom{N}{2k} = 2^{N-1}. \tag{12}$$

We must remark that one must proceed with caution when using this transfer function to analyze seismic ground motion amplification. The transfer function tends to infinity for those wavelengths for which there is a node (a point in which the amplitude of the propagating wave becomes zero due to its oscillations) at the depth of the borehole (what gives way to spurious resonances), so it should only be used if a very strong impedance contrast is known to exist at the borehole depth [2].

Expressions resembling Eq. (10) that do not employ compact notation were available in the literature [13,14]. However, the equivalent harmonic decomposition of TF^{-1}_{u-u}, Eq. (7), and the one of TF, Eq. (20) (to be introduced in the following), are novel and revealing, since they suggest that concepts borrowed from Fourier Analysis can be used to analyze transfer functions. In [8], as an example of the advantages of employing this harmonic decomposition of entries of the transfer matrix, the first author was able to identify and characterize the "building blocks" that define the dispersion relation of a modular rod in which longitudinal waves propagate. The application we study in this manuscript (HV ratios, Section 4) lends itself more naturally to be analyzed using the form Eq. (10), but we foresee tackling other problems in the future using the form in Eq. (7), see Section 5.

2.3.1. Example: $N = 2$

Let us detail how the multi-index notation unfolds to yield the well-known result [15] for the simplest possible size. For other examples of how to build expressions directly from the harmonic decomposition Eq. (7), see Ref [8]. Since $N = 2$, there can only be two multi-indices of even degree:

$$\mathsf{b} = (0,0) \to \mathrm{f}(\mathsf{b}) = (0,\,0) \to C_{(0,0)} = (-1)^0(\sqrt{\rho\mu})^{\mathsf{b}} = 1, \tag{13a}$$

$$\mathsf{b} = (1,1) \to \mathrm{f}(\mathsf{b}) = (1,\,-1) \to C_{(1,1)} = (-1)^1(\sqrt{\rho\mu})^{\mathsf{b}} = -\frac{\sqrt{\rho_1\mu_1}}{\sqrt{\rho_2\mu_2}}. \tag{13b}$$

Thus:

$$TF_{u-u}(\omega)^{-1} = \left(\prod_{i=1}^{N}\cos(r_i)\right)\left(\sum_{\beta=0}^{1}\sum_{|\beta|=2\beta} C_{\mathsf{b}}\tan(r)^{\mathsf{b}}\right) = \cos(r_1)\cos(r_2)\left(1-\sqrt{\frac{\rho_1\mu_1}{\rho_2\mu_2}}\tan(r_1)\tan(r_2)\right), \tag{14}$$

see also that the second term between parenthesis when equalized to zero provides an equation for the natural frequencies of the system, for this case and for every other number of layers greater than two.

2.3.2. Example: $N = 3$

For three layers: we have the following possible b values, which are mapped by f as

$$\mathsf{b} = (0,0,0) \to \mathrm{f}(\mathsf{b}) = (0,0,0) \to (\sqrt{\rho\mu})^{\mathsf{b}} = 1, \tag{15a}$$

$$\mathsf{b} = (1,1,0) \to \mathrm{f}(\mathsf{b}) = (1,-1,0) \to (\sqrt{\rho\mu})^{\mathsf{b}} = \frac{\sqrt{\rho_1 a_1}}{\sqrt{\rho_2 a_2}}, \tag{15b}$$

$$\mathsf{b} = (1,0,1) \to \mathrm{f}(\mathsf{b}) = (1,0,-1).\to (\sqrt{\rho\mu})^{\mathsf{b}} = \frac{\sqrt{\rho_1 a_1}}{\sqrt{\rho_3 a_3}}, \tag{15c}$$

$$\mathsf{b} = (0,1,1) \to \mathrm{f}(\mathsf{b}) = (0,1,-1) \to (\sqrt{\rho\mu})^{\mathsf{b}} = \frac{\sqrt{\rho_2 a_2}}{\sqrt{\rho_2 a_2}}, \tag{15d}$$

thus, from Eq. (10),

$$TF_{u-u}(\omega)^{-1} = \cos(r_1)\cos(r_2)\cos(r_3)\left(1-\sqrt{\frac{\rho_1\mu_1}{\rho_2\mu_2}}\tan(r_1)\tan(r_2)\right. \tag{16}$$

$$-\sqrt{\frac{\rho_1\mu_1}{\rho_3\mu_3}}\tan(r_1)\tan(r_3) - \sqrt{\frac{\rho_2\mu_2}{\rho_3\mu_3}}\tan(r_2)\tan(r_3)\Big).$$

2.4. Analytical expression for surface-to-incident-amplitude transfer function

Likewise, for P_{21} in Eq. (6) one has

$$\omega\sqrt{\rho_{half}\mu_{half}}P_{21} = \omega\left(\prod_{i=1}^{N}\cos(r_i)\right)\left(\sum_{\beta=0}^{\lfloor\frac{N-1}{2}\rfloor}\sum_{|\mathsf{b}|=1+2\beta} S_{\mathsf{b}}\tan(r)^{\mathsf{b}}\right), \tag{17}$$

the coefficients S_{b} being given by

$$S_{\mathsf{b}} = (-1)^{(|\mathsf{b}|+1)/2}(\sqrt{\rho\mu})^{\mathrm{f}(\mathsf{b})}, \tag{18}$$

since in this case the multi-index will always have degree odd, there will be an impedance that is left "hanging" (it will not enter into any impedance ratio), but it will be divided by $\sqrt{\rho_{half}\mu_{half}}$ in the final instance.

In this case, the number of addends, one can verify, is also 2^{N-1}. Combining Eqs. (17) and (10) into Eq. (6) yields the expression of the second transfer function (in similar fashion to Eq. (10)):

$$2(\mathrm{TF})^{-1} = \left(\prod_{i=1}^{N}\cos(r_i)\right)\left(\sum_{\beta=0}^{\lfloor N/2\rfloor}\sum_{|\mathsf{b}|=2\beta} C_{\mathsf{b}}\tan(r)^{\mathsf{b}} - \mathrm{i}\sum_{\beta=0}^{\lfloor\frac{N-1}{2}\rfloor}\sum_{|\mathsf{b}|=1+2\beta}\frac{S_{\mathsf{b}}}{\sqrt{\rho_{half}\mu_{half}}}\tan(r)^{\mathsf{b}}\right). \tag{19}$$

Expressing this transfer function as a harmonic decomposition, similarly to Eq. (7), is also possible:

$$\mathrm{TF}(\omega)^{-1} = \sum_{k=1}^{2^{N-1}}\left(A_k\cos\left(\tau_k\omega\right) + \mathrm{i}B_k\sin\left(\tau_k\omega\right)\right), \tag{20}$$

the spectral periods have already been introduced, Eq. (8), and the spectral amplitudes associated to the sinusoidal terms are given by

$$B_j = \frac{1}{2^N\sqrt{\rho_{half}\mu_{half}}}\sum_{k=0}^{\lfloor\frac{N-1}{2}\rfloor}\sum_{|\mathsf{b}|=2k+1}(-1)^{k+\frac{\mathsf{b}\cdot\mathbf{e}_j-1}{2}}(\sqrt{\rho\mu})^{\mathrm{f}(\mathsf{b})}. \tag{21}$$

2.4.1. Example: N = 2

For two layers, there can only be two multi-indices of odd degree:

$$\mathsf{b}=(1,0)\to\mathrm{f}(\mathsf{b})=(1,0)\to(-1)^1\tan(r_1)^1\tan(r_2)^0 S_{(1,0)} = -\sqrt{\rho_1\mu_1}\tan(r_1), \tag{22a}$$

$$\mathsf{b}=(0,1)\to\mathrm{f}(\mathsf{b})=(0,1)\to(-1)^1\tan(r_1)^0\tan(r_2)^1 S_{(0,1)} = -\sqrt{\rho_2\mu_2}\tan(r_2), \tag{22b}$$

thus, adding these terms to those obtained in Eq. (14)

$$2(\mathrm{TF}(\omega))^{-1} = \cos(r_1)\cos(r_2)\Big(1 - \sqrt{\frac{\rho_1\mu_1}{\rho_2\mu_2}}\tan(r_1)\tan(r_2) + \mathrm{i}\sqrt{\frac{\rho_1\mu_1}{\rho_{half}\mu_{half}}}\tan(r_1) + \mathrm{i}\sqrt{\frac{\rho_2\mu_2}{\rho_{half}\mu_{half}}}\tan(r_2)\Big). \tag{23}$$

Unlike the displacement–displacement transfer function, which only depends on the properties of the upper layers, in this expression the properties of the half-space do appear explicitly.

2.4.2. Example: N = 3

Likewise,

$$\mathsf{b}=(1,0,0)\to\mathrm{f}(\mathsf{b})=(1,0,0)\to-\sqrt{\rho_1\mu_1}\tan(r_1), \tag{24a}$$

$$\mathsf{b}=(0,1,0)\to\mathrm{f}(\mathsf{b})=(0,1,0)\to-\sqrt{\rho_2\mu_2}\tan(r_2), \tag{24b}$$

$$\mathsf{b}=(0,0,1)\to\mathrm{f}(\mathsf{b})=(0,0,1)\to-\sqrt{\rho_3\mu_3}\tan(r_3), \tag{24c}$$

$$\mathsf{b}=(1,1,1)\to\mathrm{f}(\mathsf{b})=(1,-1,1)\to+\sqrt{\rho_3\mu_3}\frac{\sqrt{\rho_1\mu_1}}{\sqrt{\rho_2\mu_2}}\tan(r_1)\tan(r_2)\tan(r_3), \tag{24d}$$

so adding these terms to Eq. (16)

$$\begin{aligned}TF_{u-u}(\omega)^{-1} = \cos(r_1)\cos(r_2)\cos(r_3)\Big(1 &- \sqrt{\frac{\rho_1\mu_1}{\rho_2\mu_2}}\tan(r_1)\tan(r_2) - \sqrt{\frac{\rho_1\mu_1}{\rho_3\mu_3}}\tan(r_1)\tan(r_3) - \sqrt{\frac{\rho_2\mu_2}{\rho_3\mu_3}}\tan(r_2)\tan(r_3)\\ &+\mathrm{i}\sqrt{\frac{\rho_1\mu_1}{\rho_{half}\mu_{half}}}\tan(r_1) + \mathrm{i}\sqrt{\frac{\rho_2\mu_2}{\rho_{half}\mu_{half}}}\tan(r_2) + \mathrm{i}\sqrt{\frac{\rho_3\mu_3}{\rho_{half}\mu_{half}}}\tan(r_3)\\ &-\mathrm{i}\sqrt{\frac{\rho_3\mu_3}{\rho_{half}\mu_{half}}}\sqrt{\frac{\rho_1\mu_1}{\rho_2\mu_2}}\tan(r_1)\tan(r_2)\tan(r_3)\Big).\end{aligned} \tag{25}$$

3. Verification

In order to verify the results we resort to computing numerical transfer functions (using both the conventional propagator method as outlined in Aki & Richards' "Quantitative Seismology" [1] and the method outlined in Kramer's geotechnical engineering book [2]) and comparing them to the direct evaluation of the formulas in Eqs. (3) and (4).

A list of ten Kik-net site layerings [16] has been used, the sites being those also studied in Ref. [17]. Only two examples are shown but the other eight are provided as Supplementary Material. The information about these sites, code called "TKCH08" and "NIGH11", is provided in Tables 1 and 2. Since neither damping nor density are included in the data, we choose to assign the same hysteretic damping coefficient and density value to all layers, $\delta_d = 0.1$ and $\rho = 1500\ \mathrm{kg/m^3}$.

The numerical evaluation procedure is consigned into a *Mathematica* notebook [18] that is provided to the readers, see Supplementary Material section at the end of this article. It takes advantage of the combinatorial structure of the wave propagation problem to directly generate the exact form of the transfer function in symbolic form, which is then evaluated and compared to the results of traditional direct matrix multiplication.

The comparison returns perfect agreement for both kinds of transfer functions, see Figs. 2 to 5 (in the left panel of each figure, $V_s = \sqrt{\mu/\rho}$ represents the shear wave velocity in each layer). The numerical evaluation procedure is consigned into a *Mathematica* notebook [18] that is provided to the readers, see Supplementary Material section at the end of this article.

Moreover, they allow to better understand the different shape of each kind of function: the displacement-to-displacement transfer functions do not contain odd powers of the tangents, see Eq. (10), while the displacement-to-amplitude transfer function does, Eq. (19); the latter also contains twice as many terms as the former, hence its greater shape complexity and unintuitive evolution (compare Figs. 5 to 4 and Figs. 3 to 2) should not come as a surprise.

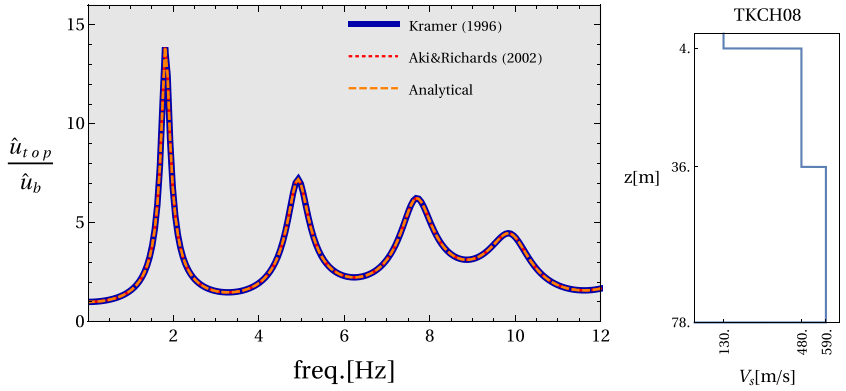

Fig. 2. Results for the surface-to-borehole transfer function between the bedrock interface and the ground surface for Kik-net station TKCH08.

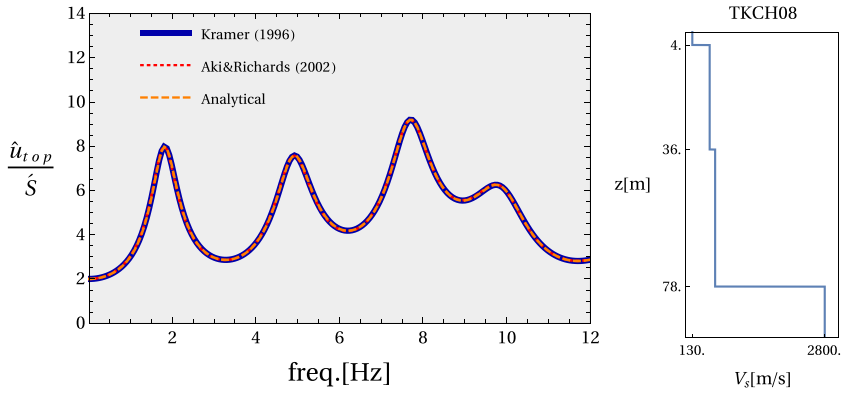

Fig. 3. Results for the surface-to-incident transfer function between the bedrock interface and the ground surface for Kik-net station TKCH08.

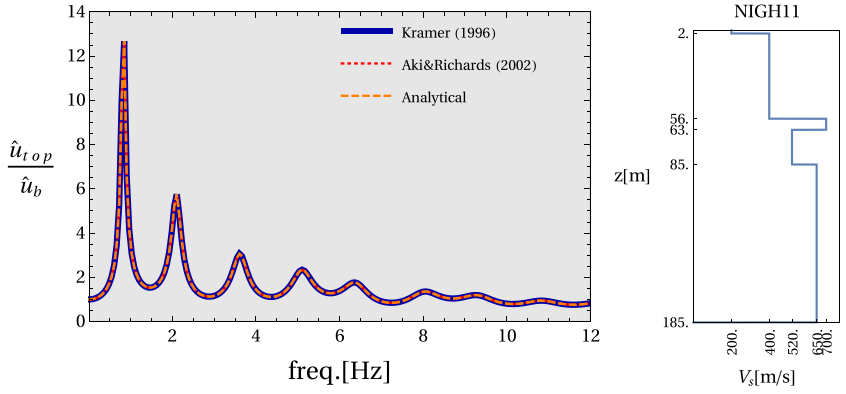

Fig. 4. Results for the surface-to-borehole transfer function between the bedrock interface and the ground surface for Kik-net station NIGH11.

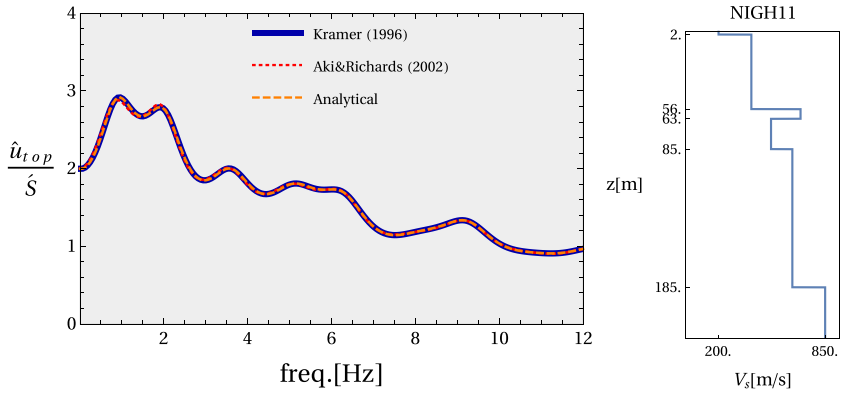

Fig. 5. Results for the surface-to-incident transfer function between the bedrock interface and the ground surface for Kik-net station NIGH11.

Table 1
Kik-net information site TKCH08.

Layer #	Thickness [m]	Depth [m]	S velocity [m/s]	P velocity [m/s]	Poisson's ratio
1	4.0	4.0	130.0	300.0	0.38
2	32.0	36.0	480.0	1850.0	0.46
3	42.0	78.0	590.0	1850.0	0.44
4	∞	∞	2800.0	5000.0	0.27

Table 2
Kik-net information site NIGH11.

Layer #	Thickness [m]	Depth [m]	S velocity [m/s]	P velocity [m/s]	Poisson's ratio
1	2.0	2.0	200.0	500.0	0.40
2	54.0	56.0	400.0	1830.0	0.47
3	7.0	63.0	700.0	1830.0	0.41
4	22.0	85.0	520.0	1830.0	0.46
5	100.0	185.0	650.0	1830.0	0.43
6	∞	∞	850.0	2080.0	0.40

4. Application: long-wavelength asymptotics of averaged horizontal-to-vertical spectral ratios

The work by Kawase, Sanchez-Sesma and Matsushima [5] outlined the relation between the surface-to-amplitude transfer functions and the H/V spectral ratio (HVSR) in the context of diffusive-field theory. The authors established a relation between the imaginary part of the Green's functions in a layered site, under the 1D linear-elastic propagation assumption, and the ratio of the horizontal spectral displacement amplitude and the vertical one. They validated the results of their development using both seismogram synthetics and real data, and proved both the convergence to their average result and its robustness (its ability to predict results also in scenarios that did not fit perfectly the assumptions used during the derivations, e.g., inclined wave field with mode conversion, a possibility that was not included in their analysis, but it was shown that the effects of this wave inclination is smoothed out by the intrinsic averaging after superimposing many cases of different inclinations).

We refer the reader to the original appear for more information concerning the limitations of the results in terms of number of records to average over, earthquake magnitude and peak ground acceleration. HVSRs are also of interest when it comes to perform inverse analysis to infer information about a site layering (soil profile) from seismic records [19,20]. Non-uniqueness of solutions is one of the fundamental challenges when solving any inverse problems, while a possible way to mitigate this issue is to enforce physics-based constraints (i.e., prior information) that any feasible solution must verify [21]. Hence, having the analytical formulae, we are now able to derive one such constraint, namely, we are to derive the exact expression for the curvature at the origin (low-frequency limit) of the averaged HVRS. In upcoming inverse analyses as the ones described in the references above, the exact expression of this parameter will provide an automatic way to discard those profiles that come up as potential solutions but do not abide by the curvature constraint.

Adopting the notation in Ref. [5], we will use TF_p to refer to P-wave transfer function (vertical displacement) while TF_s does to S-wave transfer function (horizontal one). The following relation between the ratio evaluated at the fee surface, rHV, and the displacement-to-amplitude transfer function was found:

$$\mathrm{rHV} = \frac{H(0;\omega)}{V(0;\omega)} = \sqrt[4]{\frac{8(1-\nu_{half})}{(1-2\nu_{half})}}\frac{|\mathrm{TF}_s|}{|\mathrm{TF}_p|}, \tag{26}$$

where ν_{half} represents the Poisson's ratio of the half-space material.

The result Eq. (4) provides the horizontal displacement, the vertical, invoking the 1D-propagation assumption, is obtained from the same expression, simply substituting μ by $\lambda + 2\mu$, to consider pressure wave propagation instead of shear wave.

The transfer functions that appear in Ref. [5] represent the same concepts that we have been handling in this manuscript, and hence we are in a position to offer our contribution:

It is known that the low-frequency (long-wavelength) asymptote goes to a constant value that only depends on the Poisson's ratio of the underlying half-space (in the case of it being a Poisson's solid, $\nu_{half} = 0.25$, then the asymptote is $\sqrt{2\sqrt{3}} \approx 1.86$), but, even though the asymptotic value can be computed, a general approximation of the ratio as it tends to that limit is not available and thus it must be obtained numerically along with the rest of the ratio for larger values of frequencies.

Having Eq. (19) ready, we aim to Taylor-expand it in the long-wavelength limit (i.e., around $\omega = 0$) to then use the expansion to achieve the long-wavelength asymptotic approximation of Eq. (26). We shall provide the first term of the Taylor expansion of rHV around $\omega = 0$, which happens to be the curvature at the origin (it will be shown that the initial slope is exactly zero). This formula could be used later to perform a preliminary profile inversion using averaged horizontal-to-vertical ratios at different depths before resorting to numerical computations.

First, see that in the low-frequency (long-wavelength) limit we can state that $\omega h_i/\sqrt{\mu_i/\rho_i} \ll 1$ for any $i = 1 \dots N$. This means that all the arguments of the tangents and cosines that appear in the analytical expressions, r_i for $i = 1 \dots N$, are very small, hence we consider the long-wavelength regime to correspond to $r_i \to 0$. Therefore, Eq. (10) yields

$$\lim_{r_1 \dots r_N \to 0} TF_{u-u} = 1, \tag{27}$$

while

$$\lim_{r_1 \dots r_N \to 0} \frac{P_{21}}{\omega\sqrt{\rho_{half}\mu_{half}}} = 0, \tag{28}$$

so it follows that

$$\lim_{r_1 \dots r_N \to 0} \mathrm{TF}_p = \lim_{r_1 \dots r_N \to 0} \mathrm{TF}_s = 1. \tag{29}$$

Combining, the expression of the horizontal–vertical amplitude ratio in the long-wavelength regime is finally obtained:

$$\mathrm{rHV} \approx \sqrt[4]{\frac{8(1-\nu_{half})}{(1-2\nu_{half})}}, \tag{30}$$

for $\omega \ll \min_{i=1,\dots,N}\{V_{s,i}/h_i\}$. We use V_s when stating the condition because it always holds that $V_s = \sqrt{\mu/\rho} < V_p = \sqrt{\lambda + 2\mu/\rho}$.

Additionally, the analytical formulae can also be used to estimate the gradient and the curvature of the ratio as a function of frequency in this low-frequency regime. To do so, we need to remove higher-order terms in the Taylor-expansion of the tangents and cosines around $r_i = 0$. Let us split the job and begin from Eq. (10):

$$TF_{u-u}^{-1} = \left(\prod_{i=1}^{N}\cos(r_i)\right)\left(\sum_{\beta=0}^{\lfloor N/2\rfloor}\sum_{|\mathrm{b}|=2\beta} C_{\mathrm{b}}\tan(r)^{\mathrm{b}}\right) \tag{31a}$$

$$= \left(1 - \frac{1}{2}\sum_{i=1}^{N}\left(\frac{\omega h_i}{\sqrt{\mu_i/\rho_i}}\right)^2 + \mathcal{O}(\omega^4)\right)\left(1 + \sum_{|\mathrm{b}|=2} C_{\mathrm{b}}(r)^{\mathrm{b}} + \mathcal{O}(\omega^4)\right) \tag{31b}$$

$$= 1 - \frac{1}{2}\sum_{i=1}^{N}\left(\frac{\omega h_i}{\sqrt{\mu_i/\rho_i}}\right)^2 + \sum_{|\mathrm{b}|=2}(-1)^{|\mathrm{b}|/2}(\sqrt{\rho\mu})^{\mathrm{b}'}\left(\frac{\omega h}{\sqrt{\mu/\rho}}\right)^{\mathrm{b}} + \mathcal{O}(\omega^4) \tag{31c}$$

$$= 1 - \frac{\omega^2}{2}\sum_{i=1}^{N}\left(\frac{h_i}{\sqrt{\mu_i/\rho_i}}\right)^2 - \omega^2\sum_{i=1}^{N-1}\sum_{j>i}^{N}\sqrt{\frac{\rho_i\mu_i}{\rho_j\mu_j}}\left(\frac{h_i}{\sqrt{\mu_i/\rho_i}}\right)\left(\frac{h_j}{\sqrt{\mu_j/\rho_j}}\right) + \mathcal{O}(\omega^4) \tag{31d}$$

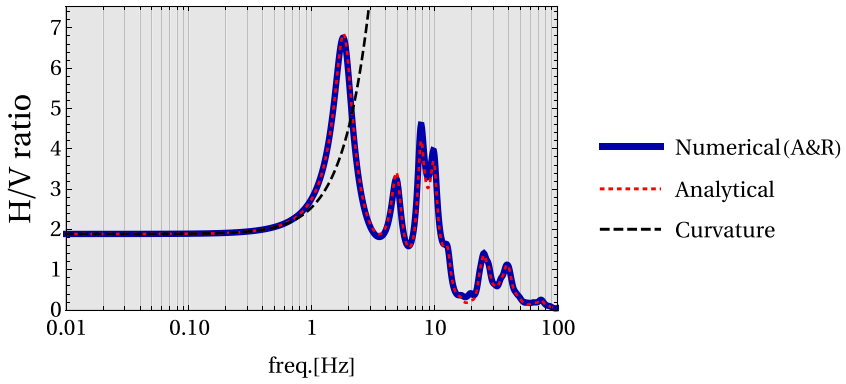

Fig. 6. Results for the horizontal-to-vertical spectral ratio for Kik-net station TKCH08.

$$= 1 - \frac{\omega^2}{2}\left(\sum_{i=1}^{N} t_i^2 + 2\sum_{i=1}^{N-1}\sum_{j>i}^{N} \mathcal{Z}_{i,j} t_i t_j\right) + \mathcal{O}(\omega^4) \tag{31e}$$

$$= 1 - \frac{\kappa}{2}\omega^2 + \mathcal{O}(\omega^4), \tag{31f}$$

where $t_i = h_i/\sqrt{\mu_i/\rho_i}$ represents the (shear) wave travel time in the ith layer, and thus

$$\kappa_s = \sum_{i=1}^{N} t_i^2 + 2\sum_{i=1}^{N-1}\sum_{j>i}^{N} \mathcal{Z}_{i,j} t_i t_j, \tag{32}$$

represents the curvature of the transfer function in the low-frequency regime, while $\mathcal{Z}_{i,j}$ represents a matrix whose entries are function of the interface impedance contrasts:

$$\mathcal{Z}_{i,j} = \prod_{k=i}^{j} Z_k, \tag{33}$$

and where, to conclude, each interface impedance contrast itself is given by

$$Z_k = \frac{\sqrt{\rho_k \mu_k}}{\sqrt{\rho_{k+1}\mu_{k+1}}}. \tag{34}$$

When it comes to deal with P waves, just substitute $\lambda + 2\mu$ in lieu of μ. Following with the second part of Eq. (6), the one that depends on P_{21}:

$$\frac{P_{21}}{\omega\sqrt{\rho_{half}\mu_{half}}} = \underbrace{\left(\prod_{i=1}^{N}\cos(r_i)\right)}_{1+\mathcal{O}(\omega^2)}\left(\sum_{\beta=0}^{\lfloor\frac{N-1}{2}\rfloor}\sum_{|\mathrm{b}|=1+2\beta}\frac{S_\mathrm{b}}{\sqrt{\rho_{half}\mu_{half}}}\tan(r)^\mathrm{b}\right) \tag{35a}$$

$$= \left(1+\mathcal{O}(\omega^2)\right)\left(\sum_{|\mathrm{b}|=1}\frac{S_\mathrm{b}}{\sqrt{\rho_{half}\mu_{half}}}(r)^\mathrm{b} + \mathcal{O}(\omega^3)\right) \tag{35b}$$

$$= \omega\sum_{|\mathrm{b}|=1}\frac{(-1)^{(|\mathrm{b}|+1)/2}(\sqrt{\rho\mu})^{\mathrm{f(b)}}}{\sqrt{\rho_{half}\mu_{half}}}\left(\frac{\omega h}{\sqrt{\rho\mu}}\right)^\mathrm{b} + \mathcal{O}(\omega^3) \tag{35c}$$

$$= -\omega\sum_{i=1}^{N}\sqrt{\frac{\rho_i\mu_i}{\rho_{half}\mu_{half}}}\left(\frac{h_i}{\sqrt{\rho_i\mu_i}}\right) + \mathcal{O}(\omega^3) \tag{35d}$$

$$= -\gamma_s\omega + \mathcal{O}(\omega^3), \tag{35e}$$

where

$$\gamma = \sum_{i=1}^{N}\mathcal{Z}_{i,N+1}t_i. \tag{36}$$

Combining the two previous results into Eq. (6) yields, finally,

$$2(\mathrm{TF}_s)^{-1} = 1 - \mathrm{i}\gamma_s\omega - \frac{\kappa_s}{2}\omega^2 + \mathcal{O}(\omega^3). \tag{37}$$

Using the latest expression, we can approximate rHV in the long-wavelength regime. Let us work with Eq. (26) squared, to ease the derivation, thus

$$\mathrm{rHV}|_{lw}^2 = \sqrt{\frac{8(1-\nu_{half})}{(1-2\nu_{half})}}\frac{\left|1-\frac{\kappa_p}{2}\omega^2 - \mathrm{i}\gamma_p\omega + \mathcal{O}(\omega^3)\right|^2}{\left|1-\frac{\kappa_s}{2}\omega^2 - \mathrm{i}\gamma_s\omega + \mathcal{O}(\omega^3)\right|^2}, \tag{38a}$$

compute the absolute value of the complex numbers by multiplying by the conjugate

$$= \sqrt{\frac{8(1-\nu_{half})}{(1-2\nu_{half})}}\frac{(1-\frac{\kappa_p}{2}\omega^2)^2 + \gamma_p^2\omega^2 + \mathcal{O}(\omega^3)}{(1-\frac{\kappa_s}{2}\omega^2)^2 + \gamma_s^2\omega^2 + \mathcal{O}(\omega^3)}, \tag{38b}$$

expanding the square in the first addends,

$$= \sqrt{\frac{8(1-\nu_{half})}{(1-2\nu_{half})}}\frac{(1-\kappa_p\omega^2 + \frac{\kappa_p^2}{4}\omega^4) + \gamma_p^2\omega^2 + \mathcal{O}(\omega^3)}{(1-\kappa_s\omega^2 + \frac{\kappa_s^2}{4}\omega^4) + \gamma_s^2\omega^2 + \mathcal{O}(\omega^3)}, \tag{38c}$$

$$= \sqrt{\frac{8(1-\nu_{half})}{(1-2\nu_{half})}}\frac{1+(\gamma_p^2-\kappa_p)\omega^2 + \mathcal{O}(\omega^3)}{1+(\gamma_s^2-\kappa_s)\omega^2 + \mathcal{O}(\omega^3)}, \tag{38d}$$

Taylor-expanding the denominator around $\omega = 0$,

$$= \sqrt{\frac{8(1-\nu_{half})}{(1-2\nu_{half})}}\left[1+(\gamma_p^2-\kappa_p)\omega^2 + \mathcal{O}(\omega^3)\right]\left[1-(\gamma_s^2-\kappa_s)\omega^2 + \mathcal{O}(\omega^3)\right], \tag{38e}$$

$$= \sqrt{\frac{8(1-\nu_{half})}{(1-2\nu_{half})}}\left\{1+\left[(\gamma_p^2-\gamma_s^2)+(\kappa_s-\kappa_p)\right]\omega^2 + \mathcal{O}(\omega^3)\right\}. \tag{38f}$$

To conclude, remove higher-order terms, square-root the prior expression and approximate it assuming the second addend is smaller than 1 to obtain:

$$\mathrm{rHV}|_{lw} = \sqrt[4]{\frac{8(1-\nu_{half})}{(1-2\nu_{half})}}\left\{1+\frac{\left[(\gamma_p^2-\gamma_s^2)+(\kappa_s-\kappa_p)\right]}{2}\omega^2\right\}. \tag{39}$$

γ_p and γ_s are the slopes of the transfer functions for P-waves and S-waves, the only difference between them that one has to use $\lambda+2\mu$ instead of μ when it comes to compute layer travel times and impedance ratios, and, likewise, κ_p and κ_s are the corresponding curvatures of the transfer functions.

The previous result indicates that the frequency plot of horizontal-to-vertical ratio should take off with zero slope but with a certain curvature. The latter asseveration appears consistent with the results in, e.g., Ref. [5] (see their images where they present HV ratios, in particular, Figures 6, 7, 8, 10, 11 and 13 in their paper).

The formula reveals that the curvature at the origin of the averaged horizontal-to-vertical ratio depends on the compressibility of the underlying halfspace through the coefficients obtained from equipartition of energy (first factor where ν_{half} appears), and through the slope and curvature at the origin of the transfer functions, which depend also on the mechanical properties of the layering up to the half-space

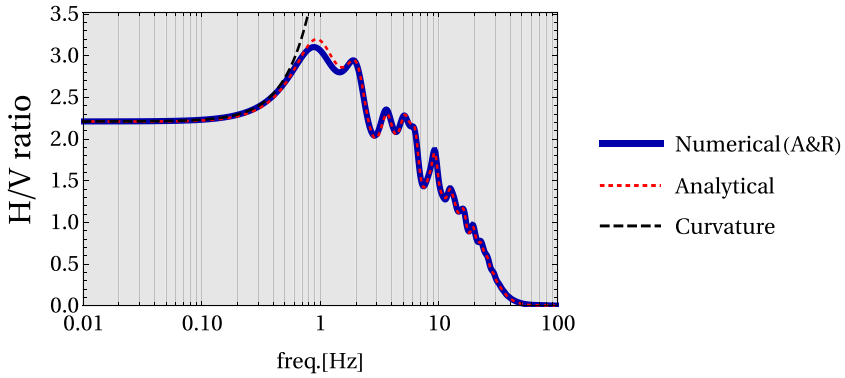

Fig. 7. Results for the horizontal-to-vertical spectral ratio for Kik-net station NIGH11.

(via the inter-layer impedances that appear in the expressions) and on the thickness of each layer (via the travel times, also present within Eqs. (32) and (36)).

Figs. 6 and 7 display, firstly, comparisons between the analytical prediction and the numerical result for the HVSR, which returns excellent agreement that does not come as a surprise since the transfer function themselves were matched perfectly in Figs. 3 and 5. Secondly and more interestingly, we can also acknowledge that the curvature is also predicted by Eq. (39): in both cases the dashed line follows the take-off of the other curves, but in one case, Fig. 6, scales slower than the actual function while in the other one rises faster than the other two curves; this indicates that the higher-order terms being ignored in Eq. (39) would be necessary to properly account for the behavior around the first peak (fundamental resonance).

5. Final remarks

The general closed-form expressions for the customary transfer functions in a 1D layered site, for any number of layers, have been introduced in this text, Eqs. (10) and (19). It has been shown that they adopt compact, manageable forms that can be expressed in terms of sums of independent harmonics, Eqs. (7) and (20). This fact may pave the way to tackle questions concerning seismic response of layered sites using an analytical approach.

These expressions allow to obtain useful information right away; in particular, we have provided the long-wavelength asymptotics of the transfer functions, and used this result to particularize the expression of the ratio of horizontal-to-vertical surface average spectral displacements, as presented in Ref. [5]. Using the closed-form expression and their long-wavelength expansions, an approximate formula of the ratio has been retrieved, see Eq. (39). The formula is valid as long as wavelengths in all layers are greater than their thickness, so it can potentially capture the behavior up to the first resonance peak. One of the interesting applications of Eq. (39) is inverse analysis: the curvature at the origin can be thought as a constraint that the real layering satisfies, so it could be used to guide the inversion of site profiles from seismic records [20].

These analytical expressions can be further explored in order to assess, for instance

- The influence of the presence of velocity reversals in a site [11].
- The definition of equivalent-homogeneous properties of inhomogeneous sites [22–25].
- The harmonic decomposition can also tell what layerings are conducive to intense ground motions, and this knowledge can in turn lead to actuations to reduce the seismic susceptibility of a site by engineering its near-surface velocity profile.

The 1D-propagation of decoupled waves is not the only wave phenomenon amenable to be treated via transfer matrices: surface waves (both Love's and Rayleigh's) and inclined bulk waves (both SH waves and P-SV waves) also lend themselves to this treatment (details on this can be found in [1]). In particular, considering inclined SH waves amounts to modifying one entry of the propagator matrix in order to introduce the ray parameter p [1], in such a case Eq. (1) would become

$$\frac{d}{dz}\begin{bmatrix}\hat{u}_y\\ \hat{\tau}_{yz}\end{bmatrix}=\begin{bmatrix}0 & 1/\mu\\ \omega^2(\mu p^2-\rho) & 0\end{bmatrix}\begin{bmatrix}\hat{u}_y\\ \hat{\tau}_{yz}\end{bmatrix}=\boldsymbol{A}\boldsymbol{f}(z), \tag{40}$$

where ρ and μ are the density and shear modulus of the layer material, and $p=\sin(\gamma)/\sqrt{\mu/\rho}$, where γ is the inclination angle with respect to the normal at the interface. Considering Love surface waves also amounts to a simple substitution in Eq. (1) [8]. This means that the understanding of these other wave propagation problems could also benefit from the knowledge of the exact form of the global propagator.

CRediT authorship contribution statement

Joaquin Garcia-Suarez: Conceptualization, Formal analysis, Writing – original draft, Validation. **Javier González-Carbajal:** Formal analysis, Validation, Writing – review & editing. **Domniki Asimaki:** Supervision, Writing – review & editing.

Declaration of competing interest

The authors declare that they have no known competing financial interests or personal relationships that could have appeared to influence the work reported in this paper.

Data availability

The data and code necessary to reproduce the results is available for download from GItHub (see Supplementary Material section of the article)

Acknowledgments

The Authors are thankful to Prof. Elnaz E. Seylabi (University of Nevada, Reno) for suggesting the application.

Appendix A. Supplementary data

Supplementary material related to this article can be found online at https://doi.org/10.1016/j.soildyn.2022.107532. A *Mathematica* notebook [18] containing the computations leading to results (including figures) shown in the text can be found in the repository named `layered_TFs` in the first author's GitHub page `github.com/jgarci-asuarez`.

A Supplementary Material document, containing a brief review of multi-index notation and results for eight more Kik-Net soil profiles, can be downloaded from the web version of this article.

References

[1] Aki K, Richards PG. Quantitative seismology. University Science Books; 2002.
[2] Kramer SL. Geotechnical earthquake engineering. in prentice–hall international series in civil engineering and engineering mechanics. Prentice Hall Inc., Englewood Cliffs, New Jersey; 1996.
[3] Gilbert F, Backus GE. Propagator matrices in elastic wave and vibration problems. Geophysics 1966;31(2):326–32.
[4] Ben-Menahem A, Singh SJ. Seismic waves and sources. Springer Science & Business Media; 2012.
[5] Kawase H, Sánchez-Sesma FJ, Matsushima S. The optimal use of horizontal-to-vertical spectral ratios of earthquake motions for velocity inversions based on diffuse-field theory for plane waves. Bull Seismol Soc Am 2011;101(5):2001–14.
[6] Morini L, Gokay Tetik Z, Shmuel G, Gei M. On the universality of the frequency spectrum and band-gap optimization of quasicrystalline-generated structured rods. Phil Trans R Soc A 2020;378(2162):20190240.
[7] Shmuel G, Band R. Universality of the frequency spectrum of laminates. J Mech Phys Solids 2016;92:127–36.
[8] Garcia-Suarez J. Harmonic decomposition of the trace of 1D transfer matrices in layered media. J Mech Phys Solids 2022;163:104830.
[9] Lekner J. Light in periodically stratified media. J Opt Soc Amer A 1994; 11(11):2892–9.
[10] Shen M, Cao W. Acoustic bandgap formation in a periodic structure with multilayer unit cells. J Phys D: Appl Phys 2000;33(10):1150.
[11] Yagoda-Biran G, Kerpel B, Kamai R. Never fear velocity ReversalsShort note. Bull Seismol Soc Am 2017;107(4):1969–74.
[12] Evans LC. Partial differential equations. Providence, R.I.: American Mathematical Society; 2010.
[13] Vinh PC, Tuan TT, Capistran MA. Explicit formulas for the reflection and transmission coefficients of one-component waves through a stack of an arbitrary number of layers. Wave Motion 2015;54:134–44.
[14] Tuan TT, Vinh PC, Ohrnberger M, Malischewsky P, Aoudia A. An improved formula of fundamental resonance frequency of a layered half-space model used in H/V ratio technique. Pure Appl Geophys 2016;173(8):2803–12.
[15] Madera GA. Fundamental period and amplification of peak acceleration in layered systems. Massachusetts research report R 70–37, MIT Press; 1970.
[16] Okada Y, Kasahara K, Hori S, Obara K, Sekiguchi S, Fujiwara H, Yamamoto A. Recent progress of seismic observation networks in Japan—Hi-net, F-net, K-NET and KiK-net—. Earth Planets Space 2004;56(8):xv–xviii.
[17] Kaklamanos J, Baise LG, Thompson EM, Dorfmann L. Comparison of 1D linear, equivalent-linear, and nonlinear site response models at six KiK-net validation sites. Soil Dyn Earthq Eng 2015;69:207–19.
[18] Wolfram S. The mathematica book, Vol. 4. Cambridge University Press Cambridge; 2000.
[19] Piña-Flores J, Perton M, García-Jerez A, Carmona E, Luzón F, Molina-Villegas JC, Sánchez-Sesma FJ. The inversion of spectral ratio H/V in a layered system using the diffuse field assumption (DFA). Geophys J Int 2016;208(1):577–88.
[20] Seylabi E, Stuart AM, Asimaki D. Site characterization at downhole arrays by joint inversion of dispersion data and acceleration time series. Bull Seismol Soc Am 2020;110(3):1323–37.
[21] Albers DJ, Blancquart P-A, Levine ME, Seylabi EE, Stuart A. Ensemble Kalman methods with constraints. Inverse Problems 2019;35(9):095007.
[22] Vrettos C. Dynamic response of soil deposits to vertical SH waves for different rigidity depth-gradients. Soil Dyn Earthq Eng 2013;47:41–50.
[23] Garcia-Suarez J, Seylabi E, Asimaki D. Seismic harmonic response of inhomogeneous soil: scaling analysis. Géotechnique 2021.
[24] Garcia-Suarez J, Seylabi E, Asimaki D. Application of ray methods to one-dimensional site response of inhomogeneous soil deposits. Géotechnique 2022;1–12.
[25] Garcia-Suarez J, Asimaki D. On the fundamental resonant mode of inhomogeneous soil deposits. Soil Dyn Earthq Eng 2020;135:106190.